Lamellar eutectic growth with anisotropic interphase boundaries

S Akamatsu, S Bottin-Rousseau, G Faivre, S Ghosh, M Plapp

Lamellar eutectic growth with anisotropic interphase boundaries

S Akamatsu[1,2], S Bottin-Rousseau[1,2], G Faivre[1,2], S Ghosh[3], M Plapp[3]

[1] CNRS, UMR 7588, INSP, 75005 Paris, France

[2] Sorbonne Universités, UPMC Univ Paris 06, UMR 7588, Institut des Nanosciences de Paris, 75005 Paris, France

[3] Condensed Matter Physics, Ecole Polytechnique, CNRS, 91128 Palaiseau, France

E-mail: akamatsu@insp.jussieu.fr

Abstract. We present a numerical study of the effect of a free-energy anisotropy of the solid-solid interphase boundaries on the formation of tilted lamellar microstructures during directional solidification of nonfaceted binary eutectic alloys. We used two different methods – phase-field (PF) and dynamic boundary-integral (BI) – to simulate the growth of periodic eutectic patterns in two dimensions. For a given Wulff plot of the interphase boundary, which characterizes a eutectic grain with a given relative orientation of the two solid phases, the lamellar tilt angle depends on the angle between the thermal axis **z** and a reference crystallographic axis. Both PF and BI results confirm the general validity of a recent approximate theory which assumes that, at the trijunctions, the surface tension vector of the interphase boundary is parallel to **z**. In particular, a crystallographic locking of the lamellae onto a direction close to a deep minimum in the Wulff plot is well reproduced in the simulations.

1. Introduction

In many nonfaceted eutectic alloys, two-phase microstructures that are delivered by coupled-growth front patterns during directional solidification (DS) present a marked morphological dependence on the crystal orientation of the two solid phases [1, 2, 3]. In spite of their pratical importance, such crystallographic effects have been largely left aside in previous theories and models. Let us consider the case of lamellar eutectics. Experimentally, it has been known for a long time that eutectic lamellae can grow tilted with respect to the thermal-gradient axis **z**, and that the lamellar tilt is eutectic-grain dependent (a eutectic grain is a region of uniform crystal orientation of the solid phases α and β [4]). On the basis of in situ experimental observations [5, 6, 7], two categories of eutectic grains have been previously distinguished (Fig. 1a), namely, *floating* (eutectic) grains (Fig. 1b1), within which the growth dynamics is well described by the standard theory of regular eutectics, and *locked* grains, within which the growth direction of the eutectic lamellae is essentially aligned to a certain crystallographic plane, and is generally inclined (or tilted) with respect to the main growth axis **z**. Lamellar patterns with a strong tilt angle are usually observed when the two solid phases exhibit an epitaxial orientation relationship and interphase-boundary planes with a low free energy [3]. Recently, an approximate theory has been formulated that relates the value of the lamellar tilt to the surface free-energy anisotropy of the α-β interphase boundaries (interfacial anisotropy) in the solid [6]. It has been proposed in coherence with in situ observations indicating that, even for lamellae that grow at a large tilt

angle, the solid-liquid interface shape exhibits a mirror symmetry with respect to the mid-plane of the lamellae, similar to the one observed for well-aligned lamellae. For isotropic solid-liquid interfaces, a symmetric shape is obtained under the condition that the contact angles of the solid-liquid interfaces at the trijunctions are the same on both sides of a lamella (Fig. 1b2) [6, 7]. For anisotropic interphase boundaries, the symmetric-pattern (SP) approximation thus entails that the Cahn-Hoffman surface tension vector $\vec{\sigma}$ [8] is aligned with $\mathbf{z}$ (it is assumed that, in a nonfaceted alloy, the anisotropy of the solid-liquid interfaces has a negligible effect on the lamellar growth dynamics).

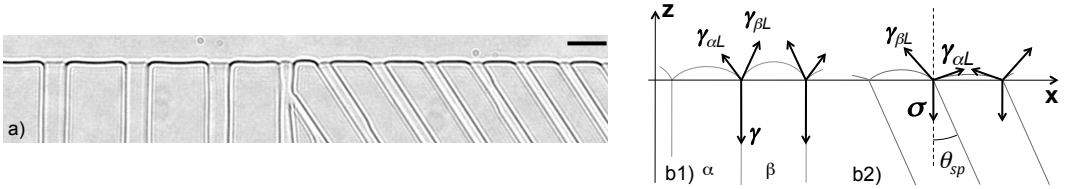

Figure 1. a) Two eutectic grains, one of the floating (lef-thand side) and the other of the locked (right-hand side) type, during real-time DS of a slightly hypoeutectic CBr_4-C_2Cl_6 alloy in a 12-μm thin sample ($V = 0.5\mu\text{ms}^{-1}$; bar: 20 μm). Sketches: b1) steady lamellar pattern with isotropic interfaces ; b2) tilted lamellar pattern in a locked eutectic grain under the SP approximation ($\vec{\sigma} \parallel \mathbf{z}$).

Here, we present a test of the SP approximation by numerical simulations. We carried out two-dimensional calculations using two different simulation methods, namely, (i) a sharp-interface code, which uses the dynamic boundary-integral (BI) formalism previously developed by Karma and Sarkissian [9], and (ii) a multi-phase-field (PF) model, based on recent grand-canonical formulations of alloy solidification [10, 11]. Both methods demonstrate that the tilt angle follows quite closely the SP approximation. In addition, a strong locking of the lamellae onto the direction of the peaked minimum of the anisotropy function is well reproduced in both BI and PF simulations.

2. The symmetric-pattern approximation

The relative orientation of the α and β crystals (constant within a grain) determines the interphase boundary free energy and its anisotropy. In two dimensions (ideally, thin-sample DS), the grain orientation and the inclination of the interphase boundary are specified each by a single angle with respect to the thermal axis. Let $\hat{n}$ be the unit normal vector of the interphase boundary, and θ the angle between $\hat{n}$ and the $\mathbf{x}$ axis ($\hat{t} = -d\hat{n}/d\theta$ is the tangent vector). For a reference grain orientation, the anisotropic interphase boundary energy is given by

$$\gamma_{\alpha\beta}(\theta) = \bar{\gamma}_{\alpha\beta} a_c(\theta), \tag{1}$$

where $\bar{\gamma}_{\alpha\beta}$ is a constant and $a_c(\theta)$ is a dimensionless function. The Cahn-Hoffman $\vec{\xi}$ and $\vec{\sigma}$ vectors [8] are defined by

$$\vec{\xi} = \gamma_{\alpha\beta}\hat{n} - \gamma'_{\alpha\beta}\hat{t} \; ; \; \vec{\sigma} = \gamma_{\alpha\beta}\hat{t} + \gamma'_{\alpha\beta}\hat{n} \tag{2}$$

where $\gamma'_{\alpha\beta} = d\gamma_{\alpha\beta}/d\theta$. The Wulff plot is given by $\vec{r}(\theta) = \gamma_{\alpha\beta}(\theta)\hat{n}$ and the minimum-energy, or Wulff shape, by the vector $\vec{\xi}(\theta)$. For a given eutectic grain, we search the steady-state growth pattern as a function of the orientation angle θ_R of the bicrystal with respect to $\mathbf{z}$. The interphase energy becomes

$$\gamma_{\alpha\beta}(\theta) = \bar{\gamma}_{\alpha\beta} a_c(\theta - \theta_R), \tag{3}$$

where $\theta_R = 0$ is chosen such that an interphase orientation of minimal energy is aligned with $\mathbf{z}$. In a sharp-interface model (with isotropic solid-liquid interfaces, and no diffusion in the solid), the local equilibrium at the trijunction is given by a Young-Herring equation, that is,

$$\gamma_{\alpha L}\hat{t}_{\alpha L} + \gamma_{\beta L}\hat{t}_{\beta L} + \vec{\sigma} = 0. \tag{4}$$

As stated above, a strictly symmetric shape is thus possible only if $\vec{\sigma}$ (which is not parallel to the interphase boundary) is aligned with $\mathbf{z}$ (Fig. 1b2), which writes

$$\gamma(\theta - \theta_R)\sin\theta + \gamma'(\theta - \theta_R)\cos\theta = 0. \tag{5}$$

For a fixed eutectic-grain orientation θ_R, this is a nonlinear equation for the interface orientation, which can easily be solved numerically for any $\gamma(\theta)$ function. We will note θ_{sp} the SP-approximation value of the tilt angle, solution of Eq. (5), and θ_t the steady-state tilt angle obtained in the numercial simulations.

3. Results and discussion

We simulated a model binary alloy with a symmetric eutectic plateau (and parallel liquidus and solidus lines), equal α- and β-liquid capillary lengths, at eutectic concentration. Temperature gradient, growth velocity, and lamellar spacing (close to the minimum undercooling spacing) are held constant. In the BI model, the interfacial anisotropy is incorporated in the calculation of the position of the trijunctions, using the Young-Herring condition (Eq. 4). In the PF model, the anisotropy of the interphase boundary is directly incorporated in the free-energy functional [11].

We implemented first a standard anisotropy function with a 4-fold symmetry [$a_c(\theta) = 1-\epsilon_4\cos 4\theta$]. The results for $\epsilon_4 = 0.04$ are shown in figure 2a. Both sets of simulation data follow quite closely the SP approximation, up to differences that do not exceed a degree. The value of θ_t passes through a maximum for an orientation that depends on the anisotropy function (as expected, symmetric, non-tilted patterns are found when either a minimum or a maximum of γ is aligned with $\mathbf{z}$). The tilt angle always remains much smaller than θ_R, which is characteristic of a weak crystallographic effect. Note that the values of the capillary length, the thermal length, and the lamellar spacing are actually slightly different for BI and PF, which demonstrates that the influence of all of these parameters is weak in realistic conditions.

We then reproduced a strong lamellar-locking effect by using an anisotropy function with a deep minimum, of the form $a_c(\theta) = 1 - \epsilon_g \exp\left[-(\theta/w_g)^2\right]$ (the smoothed gaussian cusp allows us to circumvent some obvious numerical difficulties [12]). Setting $\epsilon_g = 0.2$ and $w_g = 0.1$ entails the appearance of two (quasi) facets in the Wulff shape of the interphase boundary (see inset in Fig. 2b). In this case, the $\vec{\xi}(\theta)$ plot has self-intersections. The Wulff shape is given by the inner convex part of that plot. The other parts, often called "ears", consist of three segments delimited by turning points. The interface stiffness $\tau(\theta) = \gamma_{\alpha\beta}(\theta) + \gamma''_{\alpha\beta}(\theta)$ is negative only on the middle segment (a flat interface within this range is unstable with respect to the formation of a hill-and-valley structure [13]), but all orientations located on the "ears" are missing from the physically observable convex equilibrium shape. The SP approximation then predicts three distinct parts in the θ_{sp} vs θ_R curve: (i) an essentially linear, strongly locked branch with a slope close to 1, which runs from $\theta_R = 0$ to a first $\tau = 0$ turning point (noted θ_l); (ii) a symmetric-pattern branch along which there is no anisotropy effect for θ_R ranging from a second turning point (noted θ_u) to $\pi/2$; (iii) an intermediate, unstable branch. In the $[\theta_u, \theta_l]$ interval, two kinds of lamellar patterns (one is locked, the other is isotropic) are possible for a given eutectic-grain orientation.

Both BI and PF simulations describe the two separate branches (figure 2b) and demonstrate the existence of a strong locking effect over a large orientation range, as predicted by the SP

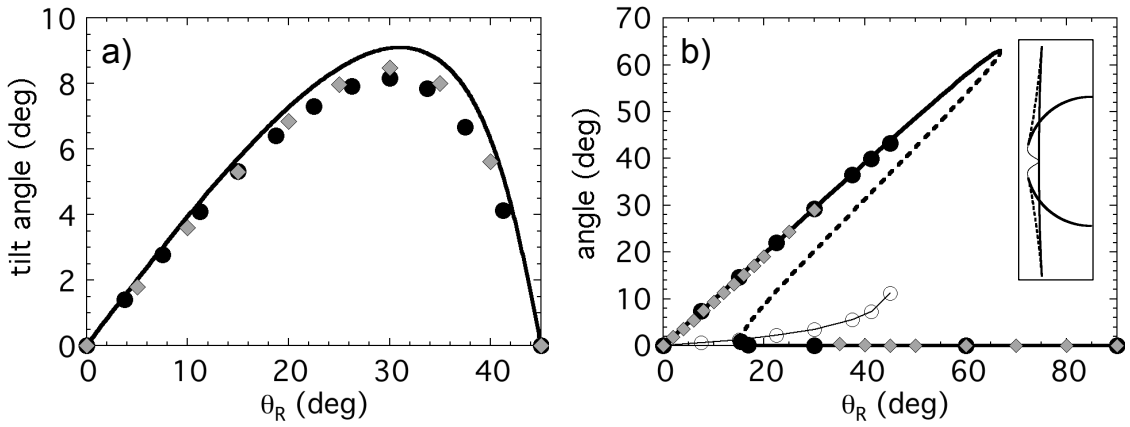

Figure 2. Lamellar tilt angle θ_{sp} predicted by the SP approximation (thick line), and θ_t calculated with the BI (filled circles) and the PF codes (diamonds) as a function of the eutectic-grain orientation angle θ_R. a) weak 4-fold anisotropy function; b) anisotropy function with a peaked gaussian minimum (see text). Open circles: angle of the surface tension vector $\vec{\sigma}$ with **z** (BI data). Inset: half view of the Wulff plot (thin line) and shape (thick line). Dotted lines: Herring-unstable orientations.

approximation. The BI simulations clearly reproduce a hysteretic behavior, which is expected for a bistable system. It should be noted, however, that the approach of the limit tilt angle (about 50 degrees) along the locked branch also corresponds to a steep, apparently diverging increase of the angle of the $\vec{\sigma}$ vector with respect to the thermal axis (Fig. 2b). This indicates that, at large tilt angles, the SP approximation, while it still correctly predicts the locked-tilt angle, becomes inaccurate with regards to other aspects of the dynamics. In contrast with the BI simulations, no hysteresis is observed in the PF simulations.

We can draw an interesting conclusion, of practical relevance, from these results. It is related to the recent development of an experimental method called *rotating directional solidification* (RDS), during which solidification is performed in a fixed thermal gradient by slowly rotating a thin alloy sample about an axis perpendicular to the **xz** plane [6, 7]. The crystal orientation of a given eutectic grain (fixed in the sample reference frame) with respect to the main solidification axis is then varied continuously while solidification proceeds. In the case of eutectic growth, a lamellar pattern then adapts its shape in a quasistationary way. It was demonstrated in Ref. [6] that, under the SP approximation, and with suitably chosen RDS settings, the solidification microstructure is then homothetic to the Wulff shape of the interphase boundaries in the sample plane, and that, accordingly, the morphological analysis of a RDS pattern gives direct access to a two-dimensional section of the corresponding Wulff plot. The present study shows that this method is accurate, within a few percents, which is quite satisfactory as compared to other ordinary sources of experimental uncertainties.

4. Conclusion

We performed time-resolved numerical simulations of tilted lamellar patterns during directional solidification of a model eutectic alloy in the presence of an anisotropy of the interphase boundaries. The simulations confirm the semi-quantitative validity of the SP approximation that assumes that the surface tension vector of the interphase boundary at the trijunctions is parallel to the main growth axis. The most salient result is that a strong locking phenomenon associated with the existence of a sharp minimum in the Wulff plot (this corresponds to a facet in the equilibrium shape of the interphase boundary) is well reproduced by the simulations.

Another interesting conclusion, of practical relevance, is the establishment of the RDS method as a good tool for extracting quantitative information on the Wulff plot of interphase boundaries during a solidification experiment. Moreover, anisotropy functions with more detailed features than the test ones used in the present work can be implemented in the simulation codes, and could serve to reproduce "real" Wulff plots measured experimentally, or calculated by molecular-dynamics methods [14]. Further simulations are planned to study the dependence of the lamellar tilt on the lamellar spacing, and the influence of a non-symmetric phase diagram. Simulations in large systems will be needed to study the dynamics of "sawtooth" patterns [5], which have been observed experimentally, and may be associated with a bistable behavior in strongly anisotropic cases. Phase-field simulations of eutectic-growth patterns with anisotropic interphase boundaries will be extended to three-dimensional, bulk-solidification geometries.

Acknowledgments
We thank Alain Karma for sharing with us his original BI code. This work was financially supported by Centre National d'Etudes Spatiales (CNES), France.

References
[1] Hogan L M, Kraft R W and Lemkey F D 1971 *Adv. Mater. Res.* **5** 8
[2] Llorca J and Orera V M 2006 *Progress in Materials Science* **51** 711
[3] Hecht U, Witusiewicz V T, Drevermann A and Rex S 2005 *Trans. Indian Inst. Met.* **58** 545
[4] Akamatsu S, Moulinet S and Faivre G 2001 *Metall Mater Trans* A **32** 2039
[5] Caroli B, Caroli C, Faivre G and Mergy J 1992 *J Cryst Growth* **118** 135
[6] Akamatsu S, Bottin-Rousseau S, Şerefoğlu M and Faivre G 2012 *Acta Materialia* **60** 3199
[7] Akamatsu S, Bottin-Rousseau S, Şerefoğlu M and Faivre G 2012 *Acta Materialia* **60** 3206
[8] Hoffmann D W and Cahn J W 1972 *Surface. Science* **31** 368
[9] Karma A and Sarkissian A 1996 *Met. Trans.* A **27** 635
[10] Plapp M 2011 *Physical Review E* **84** 031601
[11] Choudhury A and Nestler B *Physics Review E* **85** 021602
[12] Debierre J-M, Karma A, Célestini F and Guérin R 2003 *Phys Rev E* **68** 041604
[13] Herring C 1951 *Physical Review* **82** 87
[14] Kokotin V and Hecht U 2014 *Computational Materials Science* **86** 30